Available online at www.sciencedirect.com
SCIENCE DIRECT®
International Journal of Mass Spectrometry 230 (2003) 11–17
International Journal of Mass Spectrometry
www.elsevier.com/locate/ijms

A time-of-flight mass spectrometric study of laser fluence dependencies in SnO_2 ablation: implications for pulsed laser deposited tin oxide thin films

Haiyan Fan, Wei Ho, Scott A. Reid*

Department of Chemistry, Marquette University, P.O. Box 1881, Milwaukee, WI 53201-1881, USA

Received 6 May 2003; accepted 30 July 2003

Abstract

We report on a time-of-flight mass spectrometric study of laser fluence dependencies in the 532 nm ablation of SnO_2 targets. At all fluences investigated, SnO and Sn_2O_2 are the primary neutral gas-phase species. The relative yield of neutral tin-containing species increases exponentially up to a fluence of $\sim 1.9 \times 10^8$ W cm^{-2}, and saturates at higher fluences. The yield of metal oxide clusters (primarily Sn_2O_2, Sn_4O_4) increases in the saturated region, while the yield of bare metal species (primarily Sn, Sn_2) decreases. In contrast, the peak kinetic energy of the primary neutral ablated species is insensitive to laser fluence in this range. These results support the hypothesis that the initial Sn:O stoichiometry of amorphous SnO_x films grown in vacuum using pulsed laser deposition (PLD) plays an important role in the formation of α-SnO during post-deposition annealing.

Keywords: Laser; Ablation

1. Introduction

SnO_2 is a prototypical optically transparent n-type semiconductor that is widely used as a base material for the sensing of reducing gases [1–3]. Thin films have been synthesized by various means with pulsed laser deposition (PLD), a popular method [4–16]. In studies of SnO_2 films deposited on Si(0 0 1) substrates using 532 nm PLD from a compressed SnO_2 target [13,16], we found a strong correlation between deposition fluence and the phase transformations observed in post-deposition annealing. Specifically, the α-SnO phase appears only in films grown at laser fluences above $\sim 1.9 \times 10^8$ W cm^{-2}, irrespective of film thickness [16]. To understand the origin of this phenomenon, we have extended our earlier work in mass spectrometric analysis of tin oxide ablation [17,18] to examine fluence dependencies in the composition and energetics of material ablated from an SnO_2 target at 532 nm, and these results are the focus of this report. We emphasize that these experiments exclusively probe the neutral ablation pathways.

2. Experimental methods

A detailed description of the experimental apparatus may be found in [17]. Briefly, SnO_2 targets were fabricated by cold pressing SnO_2 powder (Aldrich, purity >99.9%) at a typical pressure of 6000 psi, followed by annealing at ∼1450 K for typically 60 h. The cylindrical targets were mounted on a computer controlled linear-rotary motion feedthrough that was inserted into the source region of a linear time-of-flight mass spectrometer (TOFMS). This region was evacuated by a water baffled 4 in. diffusion pump (Varian VHS-4), and the flight tube by a 250 l s^{-1} turbomolecular pump (Varian). Typical source and flight tube pressures were 3×10^{-7} and 10^{-7} mbar, respectively.

The ablation laser beam, derived from a frequency doubled Nd:YAG laser system (Continuum NY-61), was focused to a spot size of ∼1 mm diameter and struck the target along the surface normal. To ensure a constant laser spatial profile, the fluence was varied using a 532 nm λ/2 plate and thin film polarizer combination (CVI). Ablated species passed through a 3 mm aperture located ∼30 mm from the target and into the interaction region of the TOFMS, and were subsequently ionized by 118.2 nm photons generated

* Corresponding author. Tel.: +1-414-288-7565; fax: +1-414-288-7066.
E-mail address: scott.reid@mu.edu (S.A. Reid).

1387-3806/$ – see front matter © 2003 Elsevier B.V. All rights reserved.
doi:10.1016/S1387-3806(03)00344-0

by frequency tripling the 355 nm output of a second Nd:YAG laser system (Continuum Surelite II) in Xe [19]. Ions were extracted under a typical potential of 2 kV and traveled a distance of ~118 cm prior to striking a dual microchannel plate detector. The detector signal was amplified (25×) using a fast preamplifier and recorded by a multichannel scaler with a typical bin width of 5 ns. The ablation laser was triggered at 5 Hz, one-half the repetition rate of the ionization laser, affording shot-by-shot background subtraction. The typical mass resolution ($m/\Delta m$) was >200 at $m/z = 120$ amu.

Two types of data were collected. First, mass spectra were obtained over 25,000 laser shots at different laser fluences, with the delay between ablation and ionization laser initially set at 30 μs and stepped by 7 μs every 1000 shots in order to (approximately) integrate over the arrival time distribution. From these spectra the total neutral yield and relative yields of specific Sn-containing species as a function of laser fluence were obtained. Second, neutral arrival time (velocity) distributions were obtained by measuring the integrated mass signals for a given species as a function of the ablation-ionization laser delay, with the mass spectra typically accumulated over 2000 shots. Details concerning the fitting procedure are found in [17].

3. Results

We first examined the total neutral signal at a fixed neutral arrival time for all Sn-containing compounds, shown in Fig. 1 over a fluence range of $\sim 5 \times 10^7$ to 5×10^8 W cm^{-2}. The signal increases exponentially up to a fluence of $\sim 1.9 \times 10^8$ W cm^{-2}, and saturates at higher fluences. We correlate the saturation point with the onset of ablation, or formation of a laser-induced plasma, by analogy with results obtained for a Sn metal target [17], where the saturation fluence is roughly correlated with the onset of visible emission from electronically excited neutral and ionized Sn atoms, and is similar to the reported threshold for ablation at 248 nm [20].

Fig. 2 displays the fluence dependence of the fractional yields of neutral Sn-containing compounds over the same range. A consistent trend toward loss of Sn and Sn_2 is observed, with an increase in yield of Sn_2O_2 and Sn_4O_4 at higher fluence. These trends are more apparent in Fig. 3, which compares the summed data for Sn_x and Sn_xO_y species. The apparent saturation of Sn_2O_2 signal at higher fluences is artificial, since cracking of this compound to SnO is observed at higher fluences, as quantified below. We note in passing that no new species appear in the mass spectrum over this fluence range, and the day-to-day reproducibility of the data at a given fluence was within a few percent.

The laser fluence dependence of the velocity (arrival time) distributions for the dominant species, SnO and Sn_2O_2, was investigated. As shown in Fig. 4, with increasing fluence the SnO distribution increasingly deviates from a single time-transformed Maxwell–Boltzmann (MB) distribution, and the onset of this trend occurs close to the saturation point observed in Fig. 1. The distribution at 2.2×10^8 W cm^{-2} is fit reasonably well by a single MB distribution, but a close examination reveals a small contribution from a slower component, and an improved fit is obtained to a two-component MB distribution, as shown in Fig. 5a. These trends become clearer in the data obtained

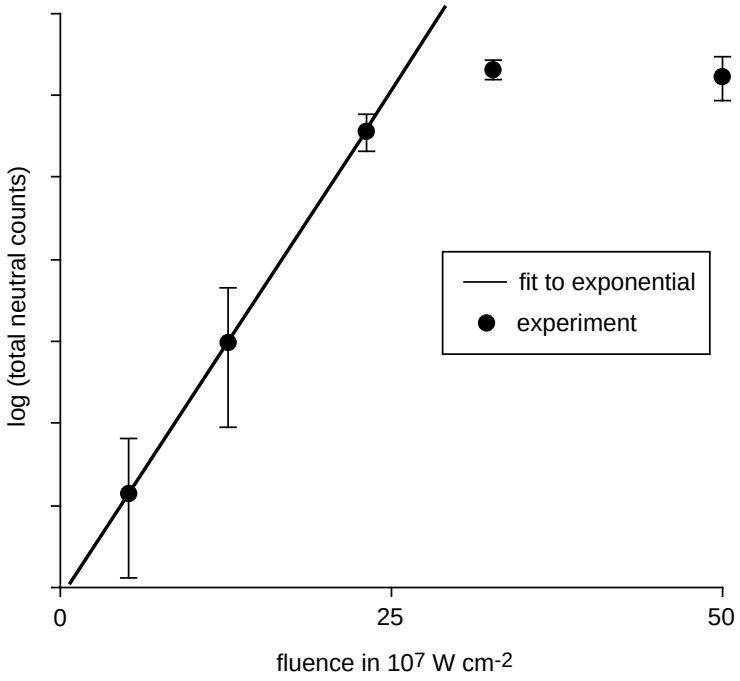

Fig. 1. Total neutral signal for all Sn-containing compounds as a function of laser fluence.

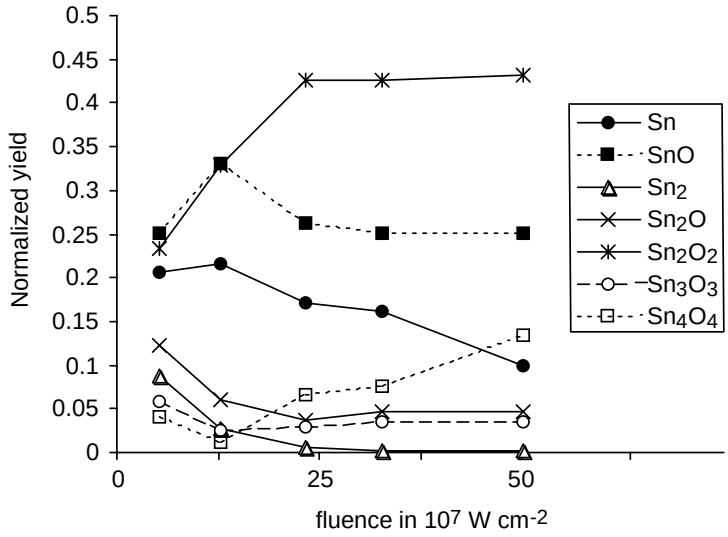

Fig. 2. Fluence dependence of the normalized yields of neutral Sn-containing species.

at 3.1×10^8 W cm^{-2}, as shown in Figs. 4 and 5b. The fit parameters obtained for the slow component are essentially identical to those for Sn_2O_2, and the Sn_2O_2 distributions at these fluences are well fit by a single MB distribution with t_{peak} set at the value obtained for the slow SnO component (Fig. 6). This result provides convincing evidence that the slow component arises from cracking of Sn_2O_2 in the ionization step, as discussed below.

Focusing on the primary component in the SnO distribution, we find a weak dependence of the peak velocity on fluence near and above the saturation point. For example, the distributions obtained at fluences of 2.2×10^8 and 3.1×10^8 W cm^{-2} give most probable speeds of 2.4×10^5 and 2.5×10^5 cm s^{-1}, respectively, with an uncertainty of 0.2×10^5 cm s^{-1}. Similarly, for Sn_2O_2 the most probable speeds at these fluences are 1.41×10^5 and 1.36×10^5 cm s^{-1}. In all cases the primary component is well fit by a single unshifted time-transformed MB distribution [17].

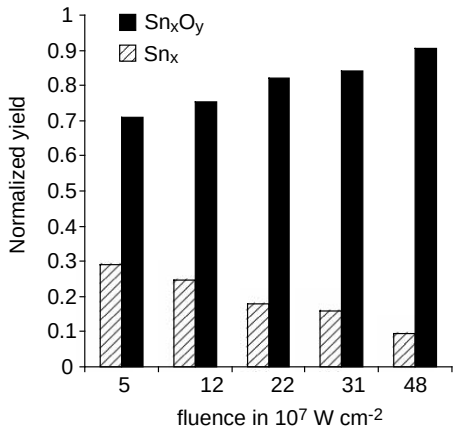

Fig. 3. Fluence dependence of the total neutral yield summed over all Sn_x and Sn_xO_y species.

4. Discussion

The major trends observed in the fluence dependence of the relative neutral yield (Fig. 2) are increases in both the yield of oxides, with concomitant loss of unoxidized species, and the yield of $(SnO)_x$ clusters with increasing fluence. A similar trend has been observed in the ablation of a La–Ca–Mn–O target [21]. We emphasize that the relative photoionization efficiencies are unknown, and thus the relative yields between species are only approximate. Moreover, the results shown in Fig. 2 were not corrected for fragmentation of Sn_2O_2 to SnO observed in the ionization step at the highest fluences, which would slightly increase the relative Sn_2O_2:SnO yield.

A decrease in relative yield for a given neutral may reflect its conversion into ions, or loss via photodissociation or secondary reactions in the gas-phase. The ionization potential of Sn (7.344 eV) is significantly smaller than that of SnO (10.5 ± 0.5 eV) [22], and the Sn_2 bond energy of 2.1 eV is also smaller than that of the oxide clusters [22]. Each of these mechanisms may therefore contribute. However, the correlation observed in yield of unoxidized versus oxidized species (Fig. 3) and the increased yield of clusters at higher fluences suggest the importance of intraplume reactions [21], which may include (thermodynamic data from [23]):

$$Sn_{(g)} + O_{2(g)} \rightarrow SnO_{(g)} + O_{(g)}, \quad \Delta H^\circ = -33.4\,\text{kJ mol}^{-1} \tag{1}$$

$$Sn_{2(g)} + O_{(g)} \rightarrow SnO_{(g)} + Sn_{(g)}, \quad \Delta H^\circ = -336.4\,\text{kJ mol}^{-1} \tag{2}$$

$$2SnO_{(g)} + M \rightarrow Sn_2O_{2(g)} + M, \quad \Delta H^\circ = -279.5\,\text{kJ mol}^{-1} \tag{3}$$

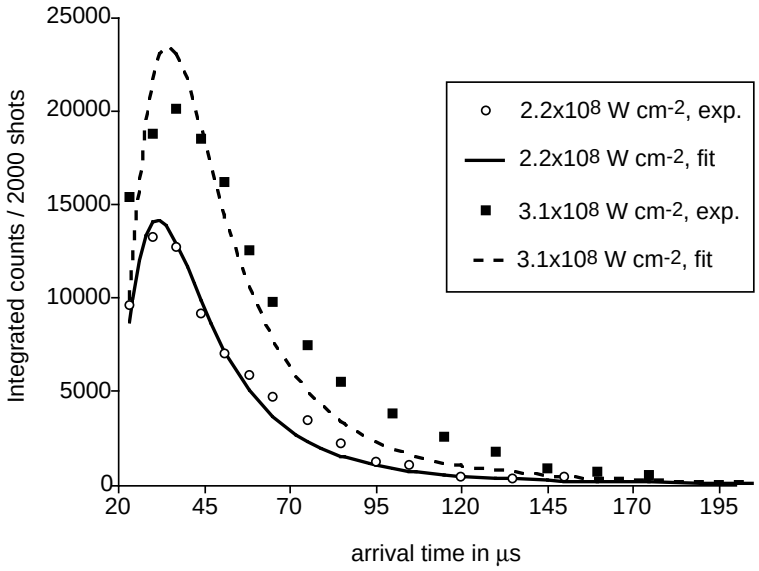

Fig. 4. SnO arrival time distributions (points) at two different laser fluences. The solid line in each plot is a fit to a single time-transformed Maxwell–Boltzmann distribution.

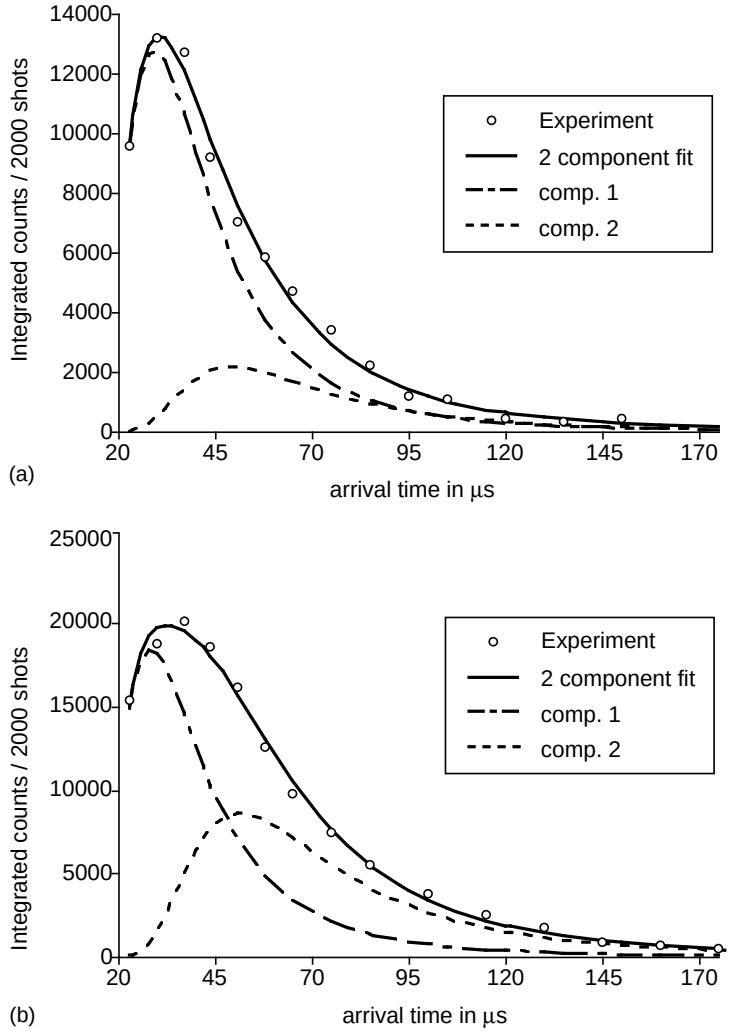

Fig. 5. SnO arrival time distributions (points) at fluences of (a) $2.2 \times 10^8\,\mathrm{W\,cm^{-2}}$ and (b) $3.1 \times 10^8\,\mathrm{W\,cm^{-2}}$. The distributions were fit to two-component time-transformed Maxwell–Boltzmann distributions, and each plot shows the two components and their sum.

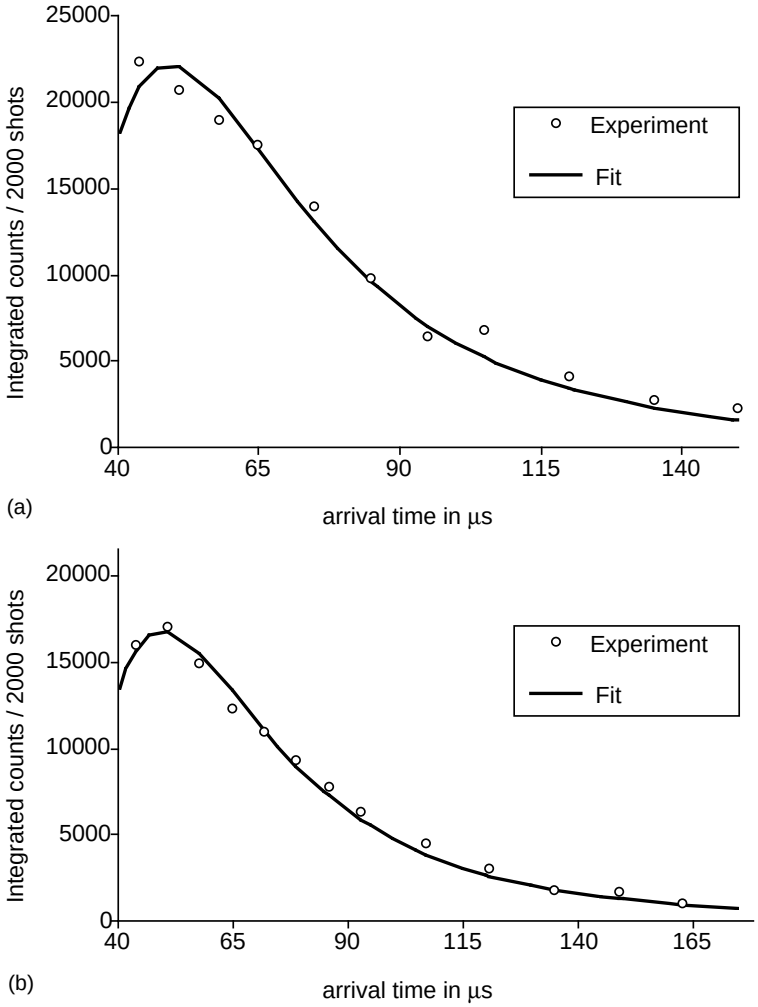

Fig. 6. Sn_2O_2 arrival time distributions (points) at fluences of (a) $2.2 \times 10^8\,W\,cm^{-2}$ and (b) $3.1 \times 10^8\,W\,cm^{-2}$. The solid line in each plot is a fit to a single Maxwell–Boltzmann distribution with t_{peak} set at the value obtained for the slow SnO component observed at the same fluence.

$$SnO_{(g)} + Sn_2O_{2(g)} + M \rightarrow Sn_3O_{3(g)} + M, \quad \Delta H^\circ = -291.6\,kJ\,mol^{-1} \tag{4}$$

$$SnO_{(g)} + Sn_3O_{3(g)} + M \rightarrow Sn_4O_{4(g)} + M, \quad \Delta H^\circ = -297.5\,kJ\,mol^{-1} \tag{5}$$

Detailed modeling of the intraplume chemistry is hampered by several factors, including our lack of knowledge of the kinetic parameters for reactions (1)–(5), and our inability to quantify the relative yields of O and O_2 [17]. However, the kinetics of reaction (1) have been measured in the temperature range 380–1840 K, and the rate constant for this spin-allowed reaction is large, approaching $2 \times 10^{-10}\,cm^3$ $molecule^{-1}\,s^{-1}$ at the highest temperatures [24,25].

As noted above, the SnO arrival time distributions become bimodal at fluences near the saturation point, and the correlation of the arrival time distribution of the slow component with that of Sn_2O_2 suggests that it arises from fragmentation of Sn_2O_2 in the ionization step, following photoionization, secondary ionization via electron impact, or interaction with residual 355 nm radiation. The former process, i.e.:

$$Sn_2O_{2(g)} + h\nu \rightarrow {Sn_2O_{2(g)}}^+ \rightarrow SnO^+_{(g)} + SnO_{(g)} \tag{6}$$

is endoergic by 3.33 eV for 118 nm photons [22], although it is possible that highly internally excited species are formed at high fluences. As a check, we investigated the arrival time distribution of Sn_4O_4 at a fluence of $4.8 \times 10^8\,W\,cm^{-2}$, as the cracking ionization of Sn_4O_4 to ${Sn_2O_2}^+$ upon electron impact has been reported [26]. The Sn_4O_4 distribution is found to peak near 110 μs, significantly slower than the primary Sn_2O_2 component. However, a small contribution from a slow component peaking near 110 μs can be seen in the Sn_2O_2 distribution obtained under the same conditions, as shown in Fig. 7, which suggests that fragmentation is occurring at higher fluences, caused either by electron impact or residual 355 nm radiation. When integrating over the arrival time distributions, the contribution of SnO signal resulting from Sn_2O_2 fragmentation was found to be 16 and 36%, respectively, at fluences of 2.2×10^8 and $3.1 \times 10^8\,W\,cm^{-2}$, and was negligible at smaller fluences.

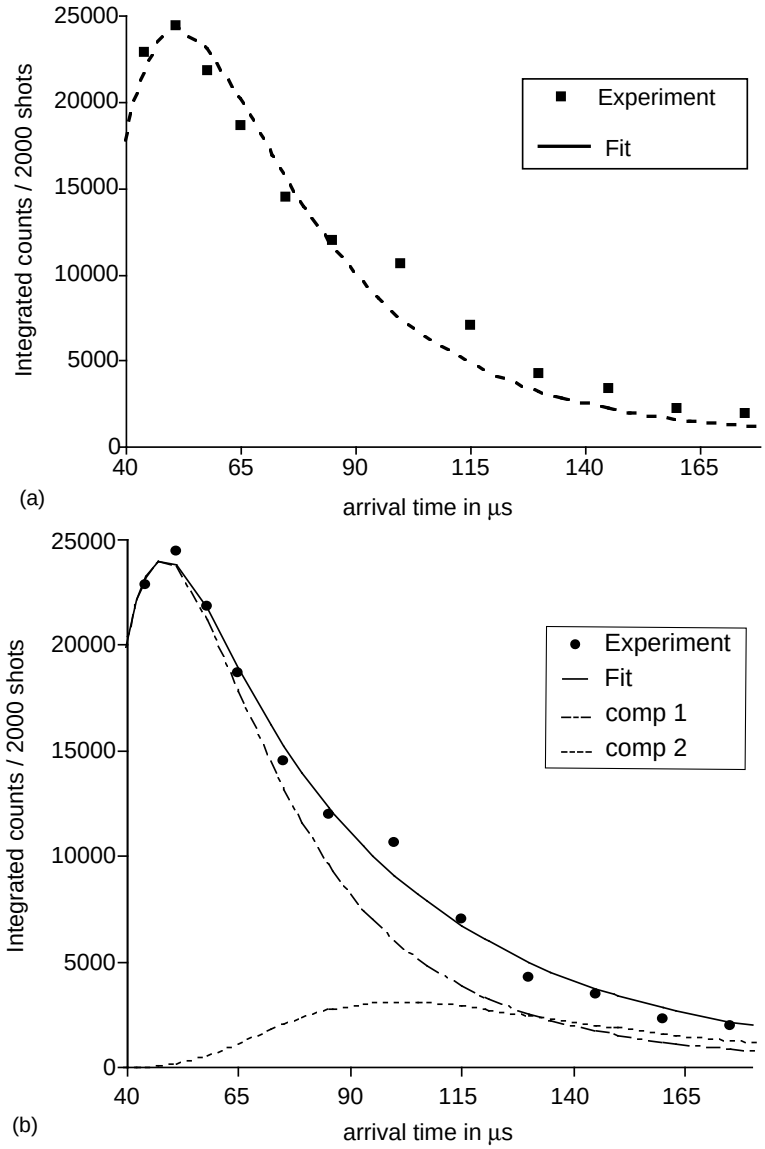

Fig. 7. Sn_2O_2 arrival time distribution at a fluence of 4.8×10^8 W cm^{-2} (points), fit to: (a) a single Maxwell–Boltzmann distribution, (b) a two-component MB distribution. The slow component has t_{peak} similar to that observed for Sn_4O_4 at the same fluence.

The primary arrival time distributions for SnO and Sn_2O_2 are well fit by unshifted time-transformed MB distributions. This cannot be taken as evidence for a thermal mechanism, as previously discussed [17]. The importance of photochemical processes is evidenced in the peak kinetic energies, which are in all cases near the ablation photon energy and exhibit a weak dependence on laser fluence.

We now turn to trends observed in PLD generated SnO_x films [13,16]. We find that, for films grown in vacuum using 532 nm PLD and subjected to post-deposition annealing in air, the formation of α-SnO is observed only for films grown at fluences above $\sim 1.9 \times 10^8$ W cm^{-2} [16]. The results presented here show that the primary effect of increasing fluence is an increase in Sn:O stoichiometry of neutral species in the plume. In contrast, the peak kinetic energies of the primary neutral species are insensitive to laser fluence in this range. These results support our initial hypothesis that the Sn:O stoichiometry of the amorphous film may govern the formation of α-SnO during post-deposition annealing [16]. Additional support is provided in the work of Muranaka et al. [27], who observed the formation of α-SnO from initially amorphous SnO_x ($x = 1.3$–1.5) films annealed in a nitrogen atmosphere. However, when the films were annealed in air, complete oxidation occurred prior to crystallization, and only r-SnO_2 (casseterite) was observed.

5. Conclusions

We have reported a time-of-flight mass spectrometric study of fluence dependencies in the 532 nm ablation of SnO_2 targets. At all fluences in the range investigated,

SnO and Sn_2O_2 are the primary neutral gas-phase species. The relative yield of neutral Sn-containing species was found to increase exponentially for pulse energies below $\sim 1.9 \times 10^8\,W\,cm^{-2}$, and saturates at higher fluences. The yield of clusters such as Sn_2O_2 and Sn_4O_4 increases in the saturated region, while the yield of unoxidized species such as Sn and Sn_2 decreases, showing that the Sn:O stoichiometry of neutral species in the plume increases at higher laser fluences. In contrast, the peak kinetic energy of the primary neutral ablated species is insensitive to laser fluence in the range investigated. These results support our hypothesis that the initial Sn:O stoichiometry of amorphous SnO_x films grown using PLD plays an important role in the formation of α-SnO during post-deposition annealing.

References

[1] M.J. Madou, S.R. Morrison, Chemical Sensing with Solid State Devices, Academic Press, Boston, 1989.
[2] H. Iida, N. Shiba, T. Mishuku, H. Karasawa, A. Ito, M. Yamanaka, Y. Haiyashi, IEEE Electron Device Lett. EDL-4 (1983) 157.
[3] K. Takahata, in: T. Seiyama (Ed.), Chemical Sensor Technology, Elsevier, Amsterdam, 1988.
[4] A.N. Shatokhin, F.N. Putilin, O.V. Safonova, M.N. Rumyantseva, A.M. Gas'kov, Inorg. Mater. 38 (2002) 374.
[5] J.E. Dominguez, X.Q. Pan, L. Fu, P.A. Van Rompay, Z. Zhang, J.A. Nees, P.P. Pronko, J. Appl. Phys. 91 (2002) 1060.
[6] W.S. Hu, Z.G. Lui, Z.C. Wu, D. Feng, Mater. Lett. 28 (1996) 369.
[7] R.D. Vispute, V.P. Godbole, S.M. Chaudhari, S.M. Kanetkar, S.B. Ogale, J. Mater. Res. 3 (1988) 1180.
[8] V.P. Godbole, R.D. Vispute, S.M. Chaudhari, S.M. Kanetkar, S.B. Ogale, J. Mater. Res. 5 (1990) 372.
[9] R. Lal, R. Grover, R.D. Vispute, R. Viswanathan, V.P. Godbole, S.B. Ogale, Thin Solid Films 206 (1991) 88.
[10] C.M. Dai, C.S. Su, D.S. Chuu, Appl. Phys. Lett. 57 (1990) 1879.
[11] N.V. Morosova, A.M. Gas'kov, T.A. Kuznetsova, F.N. Putilin, M.N. Rumyantseva, V.I. Shatnov, Inorg. Mater. 32 (1996) 292.
[12] W.S. Hu, Z.G. Liu, J.G. Zheng, X.B. Hu, X.L. Guo, W. Gopel, J. Mater. Sci. Mater. Electron. 8 (1997) 155.
[13] F.J. Lamelas, S.A. Reid, Phys. Rev. B 60 (1999) 9347.
[14] J.E. Dominguez, L. Fu, X.Q. Pan, Appl. Phys. Lett. 79 (2001) 614.
[15] X.Q. Pan, L. Fu, J.E. Dominguez, J. Appl. Phys. 89 (2001) 6056.
[16] H. Fan, S.A. Reid, Chem. Mater. 15 (2003) 564.
[17] S.A. Reid, Chem. Phys. Lett. 301 (1999) 517.
[18] S.A. Reid, W. Ho, F.J. Lamelas, J. Phys. Chem. B 104 (2000) 5324.
[19] R. Mahon, T.J. McIlrath, V.P. Myerscough, D.W. Koopman, IEEE J. Quant. Electron. QE-15 (1979) 444.
[20] R. Timm, P.R. Willmott, J.R. Huber, J. Appl. Phys. 80 (1996) 1794.
[21] H.J. Dang, Z.H. Han, Z.G. Dai, Q.Z. Qin, Int. J. Mass Spectrom. 178 (1998) 205.
[22] A.A. Radzig, B.M. Smirnov, Reference Data on Atoms, Molecules, and Ions, Springer-Verlag, Berlin, 1985.
[23] R.H. Lamoreaux, D.L. Hildenbrand, L. Brewer, J. Phys. Chem. Ref. Data 16 (1987) 419.
[24] A. Fontijn, P.N. Bajaj, J. Phys. Chem. 100 (1996) 7085.
[25] K. Takahashi, A. Giesen, P. Roth, Chem. Phys. Phys. Chem. 3 (2001) 4296.
[26] E. Zimmerman, S. Königs, D. Neuschütz, Z. Phys. Chem. 193 (1996) 195.
[27] S. Muranaka, B. Yoshichika, T. Takada, Nippon Kagaku Kaishi 11 (1987) 1886.